SUBHARMONIC IMAGING IMPLEMENTATION BY VARYING MICROBUBBLE CONCENTRATION

S. Casciaro[*,***], R. Palmizio Errico[**], F. Conversano[**], C. Demitri[**], E. Casciaro[*,***], A. Distante[*,***]

[*] National Council of Research, Institute of Clinical Physiology, Lecce, Italy
[**] ISBEM Euro Mediterranean Biomedical Scientific Institute, Brindisi, Italy

casciaro@ifc.cnr.it

Abstract: Mechanical index (MI) variations can change the nature of microbubble oscillation from linear to non linear and this has pushed the latest imaging technologies towards the development of contrast-specific harmonic modalities for the detection of flowing microbubble. The aim of this work was to define the optimal contrast agent (CA) concentration for effective harmonic imaging using low MI values. This study was carried out employing a new hydrogel-based tissue-mimicking phantom and an experimental phospholipidic microbubble CA. We used three different CA concentrations (0.033, 0.025, 0.013 μL/mL), that were insonified at fixed frequency (3.15 MHz) and variable MIs while flowing inside the phantom vessels at a constant flow rate (8 mL/min). Presented results give useful indications to choose the best imaging modality for several CA concentrations and MI value settings. Fundamental imaging resulted to be effective using a minimum MI value of 0.2 for each employed CA concentration. Harmonic imaging has been demonstrated to be employable already with MI=0.1 but this with the highest tested CA concentration; the subharmonic modality required MI=0.2 and a minimum CA concentration of 0.025 μL/mL. Several optimal settings showing imaging enhanced details are discussed and presented.

Introduction

Ultrasound (US) contrast agents (CA) have been widely used in diagnostic and therapeutic applications in medical research and clinical practice. They have been recently shown to be effective "in vitro" in US-mediated sonoporation [1-4], gene transfection [5-6] and vascular thrombosis treatment [7]. All these different and important potential future clinical applications highlight the need for having a deep knowledge of microbubble behaviour in controlled simulation, with "real" or very close to real boundary conditions, for various CA having different physical, chemical and acoustical properties. Even though CA have been already introduced in clinical routine, in fact, their potential is still far from fulfilled.

Acoustic pressure variations can change the nature of the spherical motion of a contrast bubble from linear to non linear [8] and this has moved the latest imaging technologies towards the development of contrast-specific harmonic imaging modalities for the detection of microbubbles within human body structures.

Although there are several experimental studies [9-13] showing that the acoustic pressure-dependence of microbubble backscatter is different from that of linear scatterers, the dependence of scattering behaviour of contrast microbubbles on acoustic pressure has not been the focal point in most of the previous studies and the behaviour of microbubbles in different acoustic pressure fields has not been thoroughly investigated, in particular for the last generation phospholipidic CA.

On the other hand, many discussions have been raised concerning safety in the use of microbubbles, since, at sufficient acoustic pressures, the CA gas bodies, or bubbles derived from them, can also provide nuclei for inertial cavitation [14], which is a particularly violent form of bubble activity that can damage nearby structures, even quite robust ones such as metal foils [15-18]. With the advent of gas-based CA (about fifteen years ago), it was recognized that the potential for US exposure to generate cavitation activity and bioeffects would likely be increased. This expectation was then confirmed [19] by direct and indirect evidence indicating that US-induced bioeffects attributable to the presence of microbubbles arise primarily via an inertial cavitation mechanism.

In this work we show how it is possible to reduce the inertial cavitation risk by limiting the amplitude of the employed acoustic pressure and the microbubble concentration, without loosing the diagnostic benefits of a good contrast enhancement. The purpose of this study was, in fact, to evaluate the magnitude of contrast enhanced B-mode ecographic signals, arising from a new kind of phantom, employing different mechanical index (MI) values (i.e. different values of acoustic pressure) in a range of low CA concentrations. Our final goal was the definition of the optimal combination of CA concentration and MI value for an effective and safe harmonic imaging based on a "low power technology" approach.

Materials and Methods

We performed our experiments using 3 different concentrations (0.033, 0.025, 0.013 μL/mL) of a phospholipidic microbubble CA (supplied by Bracco

ISSN: 1727-1983

Research SA, Geneva, Switzerland), whose signal intensity was evaluated at variable MI (0.08, 0.1, 0.2, 0.3). We chose just these concentration values because in a previous study [20] we demonstrated that the considered CA shows a strong linear decreasing relationship (r=0.995) between microbubble concentration and contrast intensity in the range 0.013-0.033 μL/mL.

The phantom used in this study was a custom-designed hydrogel-based tissue-mimicking phantom that contained two 1-mm diameter vessels, both placed at the same stand-off distance within the phantom (2 cm from the upper surface). The sound propagation velocity in the phantom matrix (c=1559.5 m/s) was very close to the human liver value (c=1560 m/s, [21]), while vessel walls were made of another stiffer hydrogel. A picture of the employed phantom, including a magnification of one vessel section, is reported in fig. 1.

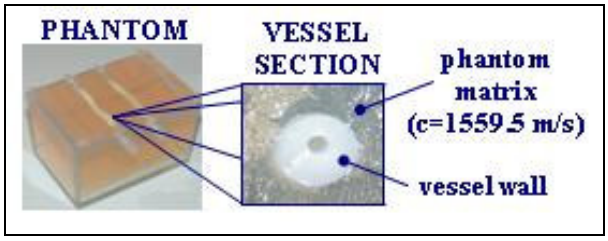

Figure 1: The employed phantom, with a magnification of one vessel section.

A linear array probe (LA 532, Esaote Spa, Florence, Italy), having a nominal center frequency of 3.15 MHz and 3-dB bandwidth 0.75 MHz, was used for US insonification with short (single-cycle) pulses. The probe was connected to a digital ecograph (Megas GPX, Esaote Spa, Florence, Italy), externally linked to a prototype for RF analysis (FEMMINA, Fast Echographic Multiparameter Multi Image Novel Apparatus, developed by Florence University), able to get the full raw signal of the probe with no hardware nor software filtering of the ecograph itself [22]. The focal point was set at 2 cm from the transducer surface (i.e. just at the vessel depth).

The three employed microbubble solutions were obtained by injecting different volumes (0.62 mL, 1.25 mL and 1.70 mL respectively) of a 1:100 saline-diluted CA sample into a continuosly stirred 500-mL saline beaker. The different solutions were then pumped at room temperature (25 °C) through the phantom vessels by a peristaltic pump (Peri-Star Model 500304, WPI Inc., FL, USA) at a constant flow rate of 8 mL/min. The transducer was positioned on the top of the phantom using a coupling gel and a shaped Plexiglas© connector as fixed reference, so that the imaging plane resulted perpendicular to the vessels. RF signals were sampled at 40 MHz (16 bits) and the number of digitized data points was 3200 for each scan line (approximately matching the phantom depth). This information was acquired for 180 scan lines in each frame.

Each employed MI value was tested with all the three CA solutions and RF raw data were acquired in sequences of 100 frames at a frame rate of about 5 frames/sec. Fortezza software (supplied by Florence University) was then used for image reconstruction and data analysis through new ad hoc implemented algorithms.

In the first step of off-line data processing, we used Fortezza software to properly choose a Region Of Interest (ROI) entirely located inside the vessel cavity. The final selected ROI included 3 scan lines and 25 data points on each scan line, which was approximately equivalent to a 0.5-mm side square.

Once the ROI had been selected, in order to evaluate the MI effect on the tested CA solutions, we implemented the Fortezza algorithm reported in figure 2, by which we calculated the Fast Fourier Transform (FFT) curve averaged over the defined ROI for each frame of every acquired sequence.

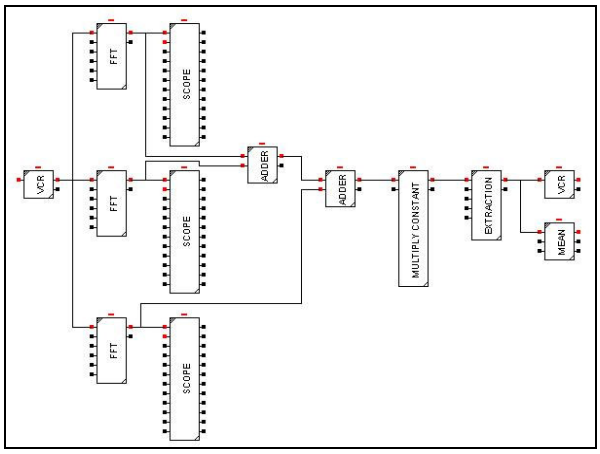

Figure 2: Fortezza algorithm used to calculate the FFT curve averaged over the selected ROI.

Looking at figure 2, the analyzed frame sequence, corresponding to a specific combination of MI and CA concentration values, was stored in the "VCR" module on the left, that, frame by frame, passed the data to the subsequent modules. Before FFT calculation, each "FFT" module selected, by means of a 25-point "Rect" window, the raw data corresponding to a different ROI scan line and zero-padded them to 4096 points to increase the frequency resolution of the spectra. FFT was calculated in this way and visualized ("SCOPE" modules, fig. 2) for every scan line of the ROI. The resulting curves were averaged (through the "ADDER" modules and the "MULTIPLY CONSTANT" module in fig. 2) in order to obtain the mean FFT curve for the selected ROI. This calculation was repeated three times for each acquired frame sequence and each time a different FFT component of the averaged FFT spectrum was extracted ("EXTRACTION" module, fig. 2), displayed ("MEAN" module, fig. 2) and recorded in a Fortezza proprietary format file ("VCR" module, fig. 2). This file was then converted in XLS format by an ad hoc implemented MATLAB® program (The

ISSN: 1727-1983

Mathworks, Inc., Natick, MA, USA); mean and standard deviation were calculated for each frame sequence by using Origin® software (OriginLab Corporation, Northampton, MA, USA) and plotted against MI value. For each tested CA concentration, we extracted from the mean FFT curve the values of the following harmonic components: fundamental (corresponding to the incident US frequency, f_0), second harmonic ($2f_0$) and subharmonic ($f_0/2$).

Results

Figures 3, 4 and 5 display the relationship between average backscatter intensity values of single FFT components and employed MI for the three considered CA concentrations.

As expected, fundamental component showed a higher intensity compared to the other components, for each tested CA concentration and for each used MI. In particular it is interesting to note that, in every reported graph, when MI increased, fundamental intensity grew with decreasing slope.

Second harmonic component exhibited a quite different behaviour: at the maximum tested CA concentration (fig. 5) second harmonic intensity showed a considerable increment when MI went from 0.08 to 0.1, while then it remained approximately constant for further MI increases. On the other hand, for lower CA concentrations (figures 3 and 4), starting from MI=0.1, when MI increased, second harmonic intensity grew more rapidly than fundamental one: in fact, when MI went from 0.1 to 0.2, second harmonic and fundamental intensities increased with about equal slopes (see figures 3 and 4), but beyond MI=0.2 second harmonic intensity continued to rise with a clearly positive slope while fundamental component seemed to have reached a kind of "plateau value" (this behaviour is particularly visible in fig. 4).

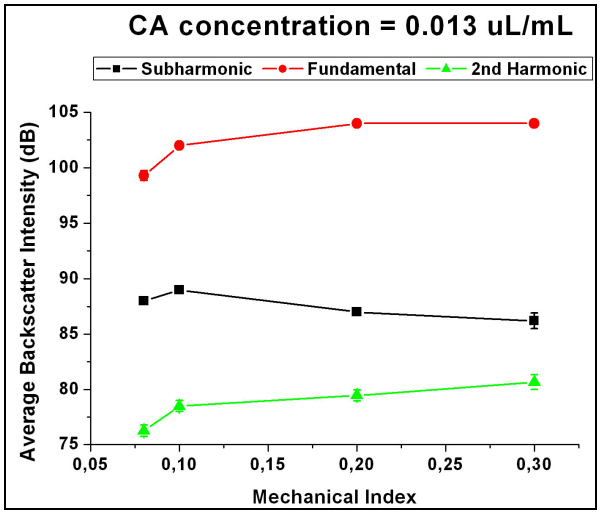

Figure 3: Plot of average backscatter intensity of single FFT components versus MI (CA concentration = 0.013 µL/mL; error bars represent standard deviations of measured data).

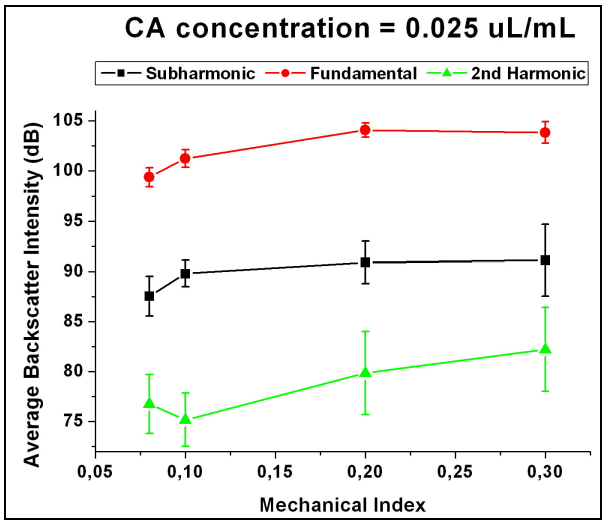

Figure 4: Plot of average backscatter intensity of single FFT components versus MI (CA concentration = 0.025 µL/mL; error bars represent standard deviations of measured data).

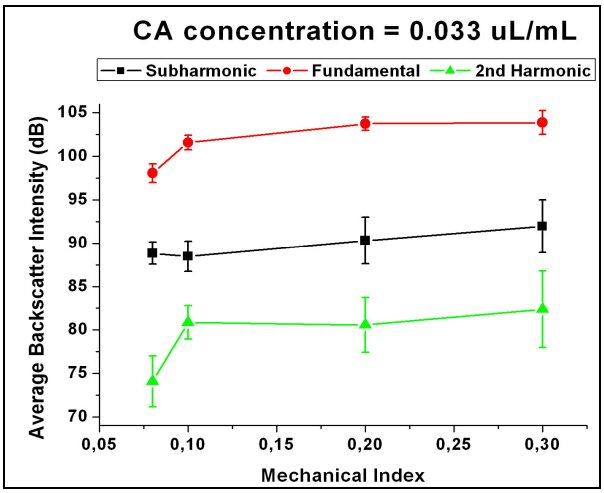

Figure 5: Plot of average backscatter intensity of single FFT components versus MI (CA concentration = 0.033 µL/mL; error bars represent standard deviations of measured data).

Finally, an interesting behaviour was showed by subharmonic component: at the lowest tested CA concentration (fig. 3) its intensity decreased with arising MI values, while at higher concentrations the observed trend became first very similar to that showed by fundamental component (fig. 4), and then, with a further increase in CA concentration, subharmonic intensity increased with an approximately constant positive slope for MI values higher than 0.1 (fig. 5).

Discussion

Backscatter intensity of single FFT components was influenced by MI variations in the considered range of CA concentrations (0.013-0.033 µL/mL).

ISSN: 1727-1983

Fundamental component showed the highest backscatter intensity for every tested combination of MI and CA concentration values, while other component curves always lay several dBs below the fundamental one. In particular, fundamental intensity showed the same trend for each employed CA concentration (see figures 3, 4 and 5), so indicating that it is more influenced by MI value rather than by CA concentration. We also noted that fundamental intensity always reached a sort of "plateau value" in correspondence of MI=0.2. This behaviour implied that, to perform an effective contrast imaging in fundamental B-mode, it should be sufficient to employ a MI of 0.2 in presence of a CA concentration of 0.013 μL/mL.

Second harmonic component presented a different trend for each CA concentration: when CA concentration was 0.013 μL/mL (fig. 3), second harmonic backscatter showed a tendency to increase proportionally to MI, but in this case the single segment slopes were lower than ones of the following graphs; in the case of CA concentration equal to 0.025 μL/mL (fig. 4), second harmonic intensity increased very rapidly when MI value went from 0.1 to 0.3; finally in presence of a CA concentration of 0.033 μL/mL (fig. 5), the curve seemed to approximately reach a "plateau value" already for MI=0.1. These results suggested that, in presence of a CA concentration of 0.033 μL/mL, second harmonic B-mode contrast imaging could be efficiently used already with a MI of 0.1, while at lower CA concentrations it should be employed a MI value of at least 0.3 with a CA concentration at least around 0.025 μL/mL. The lowest tested CA concentration (0.013 μL/mL, fig. 3), in fact, looked as if it was a too low concentration to produce useful harmonic components, at least with MI values up to 0.3.

The trend showed in figure 3 by subharmonic component intensity confirmed what has been just observed for second harmonic component: the subharmonic intensity reported in fig. 3 was even decreasing with increasing MI values, thus implying once more that a CA concentration of 0.013 μL/mL was likely to be too low for the generation of valuable harmonic components within the tested range of MI values (0.08-0.3).

On the other hand, with higher values of CA concentration, subharmonic component curves changed their shape, beginning to be increasing proportionally to MI values (see figures 4 and 5). Reported graphs suggested that subharmonic B-mode contrast imaging could be effectively implemented and used in presence of a CA concentration of 0.025 μL/mL with MI=0.2 (fig. 4), but even better results could possibly be achieved with little increments in CA concentration and MI value (fig. 5).

Conclusions

The discussed experimental measurement results gave helpful indications to choose the optimal harmonic component for B-mode contrast imaging for several combinations of MI value and CA concentrations.

Fundamental imaging resulted to be already effective with MI=0.2 in presence of a CA concentration equal to 0.013 μL/mL, and this value is likely to be even decreased through further studies aimed to explore the potential of fundamental imaging at lower microbubble concentrations.

Harmonic imaging can be efficiently employed with this phospholipidic CA with a concentration of 0.033 μL/mL and MI=0.1. Slight reductions in CA concentration are also feasible, but modest increments of MI value are simultaneously required.

Subharmonic imaging also demonstrated to be a practicable approach, being already useful with MI=0.2 and a CA concentration of 0.025 μL/mL and, moreover, showing the interesting possibility to give better intensity enhancements with the employment of slightly higher CA concentrations and MI values. In order to confirm this hypothesis, further studies are needed to fully investigate the subharmonic behaviour in a wider range of experimental settings.

Acknowledgements

We would like to thank BRACCO Research Group, Geneva, for providing us the contrast agents. We are grateful also to ESAOTE Medical systems, in particular to Giuseppe Loliva for his help and availability.

References

[1] MILLER D.L., BAO S., MORRIS J.E. (1999): 'Sonoporation of Cultured Cells in the Rotating Tube Exposure System', *Ultrasound Med Biol,* **25**, pp. 143-149

[2] WARD M., WU J., CHIU J.F. (2000): 'Experimental Study of the Effects of Optison Concentration on Sonoporation In Vitro', *Ultrasound Med Biol,* **26**, pp. 1169-1175

[3] WARD M., WU J., CHIU J.F. (1999): 'Ultrasound-Induced Cell Lysis and Sonoporation Enhanced by Contrast Agents', *J Acoust Soc Am,* **105**, pp. 2951-2957

[4] WU J., ROSS J.P., CHIU J.F. (2001): 'Reparable Sonoporation Generated by Microstreaming', *J Acoust Soc Am,* **110**, pp. 1460-1464

[5] FRENKEL P.A., CHEN S., THAI T., SHOET R.V., GRAYBURN P.A. (2002): 'DNA-Loaded Albumin Microbubbles Enhance Ultrasound-Mediated Transfection In Vitro', *Ultrasound Med Biol,* **28**, pp. 817-822

[6] GREENLEAF W.J., BOLANDER M.E., SARKAR G., GOLDRING M.B., GREENLEAF J.F. (1998): 'Artificial Cavitation Nuclei Significantly Enhance Acoustically Induced Cell Tranfection', *Ultrasound Med Biol,* **24**, pp. 587-595

[7] UNGER E.C., MATSUNAGA T.O., MCCREERY T., SCHUMANN P., SWEITZER R., QUIGLEY R. (2002): 'Therapeutic Applications of Microbubbles', *Eur J Radiol,* **42**, pp. 160-168

ISSN: 1727-1983

[8] DE JONG N. (1993): 'Acoustic Properties of Ultrasound Contrast Agents' (PhD Thesis)
[9] KRISHNA P.D. and NEWHOUSE V.L. (1997): 'Second Harmonic Characteristics of the Ultrasound Contrast Agents Albunex and FSO69', *Ultrasound Med Biol,* **23**, pp. 453-459
[10] MORGAN K.E., DAYTON P.A., KRUSE D.E., KLIBANOV A.L., BRANDENBURGER G.H., FERRARA K.W. (1998): 'Changes in the Echoes from Ultrasonic Contrast Agents with Imaging Parameters', *IEEE Trans UFFC,* **45**, pp. 1537-1548
[11] SHI W.T., FORSBERG F., RAICHLEN J.S., NEEDLEMAN L., GOLDBERG B.B. (1999): 'Pressure Dependence of Subharmonic Signals from Contrast Microbubbles', *Ultrasound Med Biol,* **25**, pp. 275-283
[12] SHI W.T. and FORSBERG F. (2000): 'Ultrasonic Characterization of the Nonlinear Properties of Contrast Microbubbles', *Ultrasound Med Biol,* **26**, pp. 93-104
[13] FRINKING P.J.A. and DE JONG N. (1998): 'Acoustic Modelling of Shell-Encapsulated Gas Bubbles', *Ultrasound Med Biol,* **24**, pp. 523-533
[14] CHEN W.S., BRAYMAN A.A., MATULA T.J., CRUM L.A. (2003): 'Inertial Cavitation Dose and Hemolysis Produced In Vitro with or without Optison', *Ultrasound Med Biol,* **29**, pp. 725-737
[15] BAILEY M.R., BLACKSTOCK D.T., CLEVELAND R.O., CRUM L.A. (1999): 'Comparison of Electrohydraulic Lithotripters with Rigid and Pressure-Release Ellipsoidal Reflectors. II. Cavitation Fields', *J Acoust Soc Am,* **106**, pp. 1149-1160
[16] COLEMAN A.J., SAUNDERS J.E., CRUM L.A., DYSON M. (1987): 'Acoustic Cavitation Generated by an Extracorporeal Shockwave Lithotripter', *Ultrasound Med Biol,* **13**, pp. 69-76
[17] CRUM L.A. (1988): 'Cavitation Microjets as a Contributory Mechanism for Renal Calculi Disintegration in ESWL', *J Urol,* **140**, pp. 1587-1590
[18] SOKOLOV D.L., BAILEY M.R., CRUM L.A. (2001): 'Use of a Dual-Pulse Lithotripter to Generate a Localized and Intensified Cavitation Field', *J Acoust Soc Am,* **110**, pp. 1685-1695
[19] AIUM (AMERICAN INSTITUTE OF ULTRASOUND IN MEDICINE) (2000): 'Mechanical Bioeffects from Diagnostic Ultrasound: AIUM Consensus Statements. Section 6 – Mechanical Bioeffects in the Presence of Gas-Carrier Ultrasound Contrast Agents', *J Ultrasound Med,* **19**, pp. 120-142
[20] CASCIARO S., PALMIZIO ERRICO R., CONVERSANO F., MAFFEZZOLI A., SANNINO A., DISTANTE A. (2005): 'Ultrasound Signal Enhancement Varying Microbubble Concentration at Very Low Mechanical Indices', Proc. of NBC'05 – 13th Nordic Baltic Conf. on Biomed. Eng. and Med. Phys. Umeå, Sweden, 2005, p. 109-110
[21] BAZZOCCHI M. (2001): 'Ecografia', II edition. (Idelson Gnocchi Editor)
[22] SCABIA M., BIAGI E. and MASOTTI L. (2002): 'Hardware and software platform for real-time processing and visualization of echographic radiofrequency signals', *IEEE Trans UFFC*, **49**, pp. 1444-1452

ISSN: 1727-1983